UNIVERSITY OF COPENHAGEN

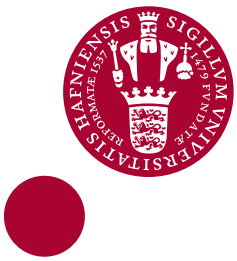

Geodetic and model data reveal different spatio-temporal patterns of transient mass changes over Greenland from 2007 to 2017

Zhang, Bao; Liu, Lin; Khan, Shfaqat Abbas; Dam, Tonie van; Bjørk, Anders Anker; Peings, Yannick; Zhang, Enze; Bevis, Michael; Yao, Yibin; Noël, Brice

Published in:
Earth and Planetary Science Letters

DOI:
10.1016/j.epsl.2019.03.028

Publication date:
2019

Document version
Publisher's PDF, also known as Version of record

Document license:
CC BY-NC-ND

Citation for published version (APA):
Zhang, B., Liu, L., Khan, S. A., Dam, T. V., Bjørk, A. A., Peings, Y., Zhang, E., Bevis, M., Yao, Y., & Noël, B. (2019). Geodetic and model data reveal different spatio-temporal patterns of transient mass changes over Greenland from 2007 to 2017. *Earth and Planetary Science Letters*, *515*, 154-163. https://doi.org/10.1016/j.epsl.2019.03.028

Download date: 04. May. 2023

Earth and Planetary Science Letters 515 (2019) 154–163

Contents lists available at ScienceDirect

Earth and Planetary Science Letters

www.elsevier.com/locate/epsl

Geodetic and model data reveal different spatio-temporal patterns of transient mass changes over Greenland from 2007 to 2017

Bao Zhang [a,b,*], Lin Liu [b], Shfaqat Abbas Khan [c], Tonie van Dam [d], Anders Anker Bjørk [e], Yannick Peings [f], Enze Zhang [b], Michael Bevis [g], Yibin Yao [a], Brice Noël [h]

[a] School of Geodesy and Geomatics, Wuhan University, Wuhan, China
[b] Earth System Science Programme, The Chinese University of Hong Kong, Shatin, Hong Kong
[c] DTU Space-National Space Institute, Technical University of Denmark, Department of Geodesy, Kgs. Lyngby, Denmark
[d] Faculty of Science, Technology, and Communication, University of Luxembourg, Luxembourg City, Luxembourg
[e] Centre for GeoGenetics, Natural History Museum of Denmark, University of Copenhagen, Copenhagen, Denmark
[f] Department of Earth System Science, University of California, Irvine, Irvine, CA, USA
[g] School of Earth Science, The Ohio State University, OH, USA
[h] Institute for Marine and Atmospheric Research, Utrecht University, Utrecht, the Netherlands

ARTICLE INFO

Article history:
Received 13 November 2018
Received in revised form 29 January 2019
Accepted 18 March 2019
Available online 29 March 2019
Editor: R. Bendick

Keywords:
Greenland
transient mass change
GRACE
GPS
SMB
ice discharge

ABSTRACT

Much of the research to understand the ice mass changes of Greenland ice sheet (GrIS) has focused on detecting linear rates and accelerations at decadal or longer periods. The transient (short-term, non-secular) mass changes show large variability, and if not properly accounted for, can introduce significant biases into estimates of long-term ice mass loss rates and accelerations. Despite the growing number of geodetic observations, in terms of spatial coverage, types of observables, and the extent of the time series, studies of the transient mass changes over GrIS are lacking. To address this limitation, we apply multi-channel singular spectral analysis to the Gravity Recovery and Climate Experiment (GRACE) mass concentrations (mascon), surface mass balance (SMB) model output, and ice discharge data, to determine the transient mass changes over Greenland over the decade (2007 to 2017). The goal of this analysis is to elucidate the spatio-temporal variability of the ice mass change. For the entire GrIS, both the mascon and SMB transient mass changes are characterized by a sustained mass gain from late 2007 to early 2010, a sustained mass loss from early 2010 to early 2013, and a mass gain from early 2013 to mid-2015. Global Positioning System sites deployed along the coast of Greenland showed uplift from early 2010 to early 2013 and subsidence from early 2013 to 2015, consistent with the corresponding ice mass loss and gain of the entire GrIS. The peak-to-peak amplitude of the transient mass change was estimated to be -294 ± 27 Gt from GRACE mascons and -252 ± 16 Gt from the SMB where the latter value includes the effect of ice discharge. The transient mass change due to ice discharge accounted for less than 10% of the total transient mass change. Our regional assessment reveals that the central-west, southwest, northeast, and southeast regions display similar time-varying patterns as we found for the entire GrIS, but the north and northwest regions show different patterns. Atmospheric circulation anomalies as measured by the Greenland Blocking Index (GBI) are able to explain most of these transient anomalies. More specifically, high-GBI-associated high temperature was one of the main reasons for the transient mass loss of the entire GrIS during 2010-2012 while low GBI can explain the transient mass gain during 2013-2015. Contrasting behaviors of precipitation anomalies in east and west Greenland under abnormally high or low GBI conditions may explain the different patterns of the transient mass change in the northwest and the rest of Greenland.

© 2019 The Author(s). Published by Elsevier B.V. This is an open access article under the CC BY-NC-ND license (http://creativecommons.org/licenses/by-nc-nd/4.0/).

1. Introduction

Over the past two decades, ice loss from the Greenland ice sheet (GrIS) has accelerated, making Greenland one of the largest contributors to sea level rise (Cazenave and Remy, 2011; Khan et al., 2014). This long-term acceleration was accompanied by short-

* Corresponding author at: School of Geodesy and Geomatics, Wuhan University, Wuhan, China.
E-mail addresses: sggzb@whu.edu.cn (B. Zhang), liulin@cuhk.edu.hk (L. Liu), abbas@space.dtu.dk (S.A. Khan), tonie.vandam@uni.lu (T. van Dam), andersb@snm.ku.dk (A.A. Bjørk), ypeings@uci.edu (Y. Peings), mbevis@osu.edu (M. Bevis), B.P.Y.Noel@uu.nl (B. Noël).

https://doi.org/10.1016/j.epsl.2019.03.028
0012-821X/© 2019 The Author(s). Published by Elsevier B.V. This is an open access article under the CC BY-NC-ND license (http://creativecommons.org/licenses/by-nc-nd/4.0/).

term highly dynamic fluctuations in space and time (Wouters et al., 2008; Chen et al., 2011; Seo et al., 2015; Khan et al., 2014) that introduces uncertainties in predictions of future ice loss. This is particularly the case over the past decade when the Greenland Blocking Index (GBI) was more frequently at extreme levels than before (Hanna et al., 2016). The accompanying atmospheric circulation anomalies exerted great impacts on Greenland ice mass balance. Therefore, it is necessary to thoroughly investigate the short-term ice mass change patterns over Greenland from the past decade and their links with the atmospheric circulation anomalies.

Most studies have focused on the long-term ice mass loss of the GrIS (e.g., van den Broeke et al., 2009; Zwally et al., 2011; Shepherd et al., 2012; Kjeldsen et al., 2015; Khan et al., 2016). Others also studied the short-term ice mass changes and their impacts on estimates of long-term ice mass loss (Velicogna et al., 2005; Velicogna and Wahr, 2006; Chen et al., 2006; Ramillien et al., 2006; Wu et al., 2006; Velicogna, 2009; Csatho et al., 2014). GRACE has been particularly valuable in determining non-secular mass changes (Velicogna et al., 2005; Wouters et al., 2008; Chen et al., 2011). Sasgen et al. (2012) combined GRACE data with Interferometric Synthetic Aperture Radar, and regional climate model data to investigate the GrIS ice mass loss and found that the ice discharge, surface melting, runoff, and precipitation contributed to the ice mass balance in a complex and regionally-variable interplay. Csatho et al. (2014) used altimetry data from 1993 to 2012 to reveal the complex spatio-temporal variations of dynamic mass loss and widespread intermittent thinning.

None of the above listed studies characterized and explained the most recent spatio-temporal short-term mass changes over the entire GrIS. With the increasing number of geodetic observations, it is time to conduct a systematic, comprehensive, and up-to-date investigation of these data to address this problem. Since the long-term and seasonal mass changes in Greenland have been well studied, in this study we will focus on the transient mass changes, i.e., ~3-year changes.

To understand the spatiotemporal characteristics of the transient ice mass changes over Greenland, multiple datasets are used. GRACE mascon data are used to investigate the transient ice mass changes over the entire GrIS as well as the spatial variability over the different sub-regions. Global Positioning System (GPS) vertical displacements are used to investigate the bedrock's elastic response to ice loading changes and further constrain the estimates of ice mass changes. The transient ice mass changes due to surface mass balance (SMB) and ice discharge are also modeled and compared with the GRACE results. Finally, we also explore the possible links between the transient ice mass changes and atmospheric circulation anomalies represented by GBI.

2. Data

2.1. GRACE data

We use GRACE mascon solutions from Jet Propulsion Laboratory (JPL), Goddard Space Flight Center (GSFC), and the Center for Space Research (CSR), University of Texas Austin. Hereafter, we refer to them as the "JPL mascon", "GSFC mascon", and "CSR mascon", respectively. The JPL mascon is the release 5 version 2 with the coastal resolution improvement filter (Wiese, 2015). The GSFC mascon is the release 5 version 2.3b (Luthcke et al., 2013; Watkins et al., 2015;). The CSR mascon is the release 5 version 1.0 (Save et al., 2016). To account for the land/ocean mass leakage, we follow Save et al. (2016) to extend the coastlines of Greenland by 120 km into the ocean. Based on these new boundaries and the drainage basins defined by Rignot et al. (2011), we divide Greenland into 6 sub-regions: 'NO' (north), 'NW' (northwest), 'CW' (central-west), 'SW' (southwest), 'NE' (northeast), and 'SE' (southeast), which are shown in Fig. 1.

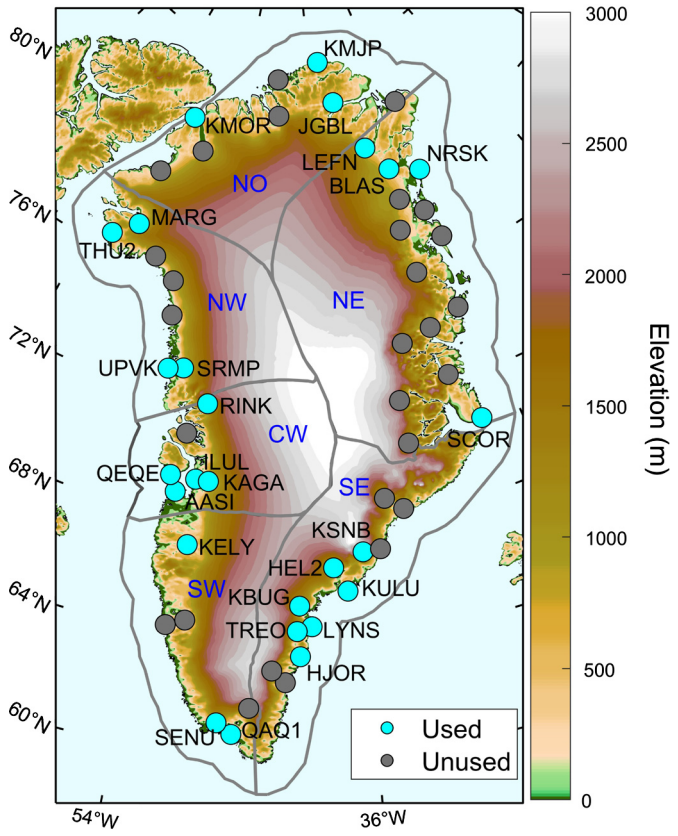

Fig. 1. GPS sites (circles filled with gray or cyan) and six sub-regions (delineated by gray lines) in Greenland. The cyan sites are used in this study. The gray sites are not used due to data gaps or their short time duration. (For interpretation of the colors in the figure(s), the reader is referred to the web version of this article.)

After obtaining the mass change time series for each sub-region, we interpolate them to monthly data with equal spacing using spline interpolation. We then fit and remove the linear and quadratic terms from the interpolated time series to obtain the detrended time series. Hereafter, we refer to this mascon residual time series as the "mascon data".

2.2. SMB and ice discharge data

SMB and ice discharge to the ocean are the two ways that the GrIS losses ice mass. SMB is the difference between accumulation from precipitation (snow and rain) and mass loss from ablation (melting, sublimation, evapotranspiration, and runoff). SMB outputs by the regional climate model, MAR version 3.8 (Fettweis et al., 2017, updated in 2018) and RACMO2.3p2 (Noël et al., 2018) are used in this study. The MAR output data are provided at monthly for 5 × 5 km grids over the entire GrIS. The RACMO2.3p2 provides 1×1 km monthly incremental SMB covering the whole GrIS and peripheral ice caps and 5.5 × 5.5 km monthly cumulative precipitation, sublimation, and runoff covering the surrounding tundra region. We obtain the RACMO2.3p2 SMB over tundra by using precipitation minus ablation from sublimation and runoff. Compared to the data described in Noël et al. (2018), no model physics has been changed. Only the spatial resolution has been increased to 5.5 km from 11 km. To obtain the SMB over the sub-regions, we integrate the monthly incremental SMB at each grid point and then sum the values of all points within each sub-region. We fit and remove the linear and quadratic terms from each SMB time series

to obtain the residual data that will be referred to as "SMB data" hereafter.

We also use the ice discharge data over Greenland from Bamber et al. (2018) to account for the mass changes due to glacier dynamics. This new data set provides data from 1958 to 2016 by supplementing and extending Rignot et al. (2008) with a new data set that captures surface velocities at sub-annual temporal intervals for 195 outlet glaciers across Greenland. We calculate the total ice discharge from the entire GrIS and from each sub-region. We also fit and remove the linear and quadrative terms from each ice discharge time series to obtain the residual data, termed as "dynamics data" hereafter.

2.3. GPS data

There are more than 50 GPS receivers sited around the edge of the GrIS, most of which were deployed after 2006 as part of the Greenland network, GNET (Fig. 1). The GPS raw data are processed by the same software and settings as detailed in Khan et al. (2010) to yield daily coordinate solutions and their uncertainties in the International Global Navigation Satellite System Service 2008 (IGS08) frame. In this study, we use only the vertical coordinate time series. We do not use the GPS sites that began collecting data after 2009.0 or those that experienced extreme data gaps between 2010 and 2013 as these data deficiencies will impact the determination of the main features of the transient displacements. In total, we use 26 sites that are shown in Fig. 1.

The vertical displacements of these sites represent the bedrock's response to historical and present surface mass changes and can be used to infer the ice mass changes (Khan et al., 2010; Wahr et al., 2013). As we focus on the displacement caused by ice loading, we follow Zhang et al. (2017, 2018) to calculate and remove the atmospheric, hydrologic, and non-tidal ocean loading displacements using the Green's function method (Farrell, 1972). We fit and remove the linear and quadratic terms from the vertical position time series to obtain the residual time series. A singular spectral analysis (SSA) method is used to fill the data gaps. The post-processed GPS vertical position time series are simply called as "GPS data" hereafter.

3. Extracting the transient signal

Multi-channel Singular Spectral Analysis (M-SSA) is an advanced data-adaptive method that detects various signals by simultaneously taking advantage of the spatial and temporal correlations in geophysical fields (Broomhead and King, 1986). It does not require a priori information on mathematical function or stochastic model, making it suitable for analyzing various kinds of data. Based on these advantages we choose M-SSA to extract the transient signals from the GRACE mascon data, the SMB data, the ice discharge data, and the GPS data. This approach has been proven effective in detecting and reconstructing periodic and non-periodic signals from noisy GPS and GRACE time series (Rangelova et al., 2012; Walwer et al., 2016; Zhang et al., 2017, 2018). We use the same M-SSA methods and settings as used in Zhang et al. (2017). Readers may refer to Zhang et al. (2017) and Section S1 of the Supplementary Material (SM) for further details.

We apply M-SSA to the mascon time series of the six subregions simultaneously to extract the transient signals of ice mass changes using the JPL, CSR, and GSFC mascons. In Section S1 of the SM we provide the technical details of how we retrieve the transient signals and we show the first ten reconstructed components of the M-SSA results. We average the transient signals from the JPL, GSFC, and CSR mascons and use this average as the final transient signal. The largest differences between the average transient signal and the three individual transient signals are regarded as the uncertainties. We apply the same procedure to the SMB and ice discharge data, to retrieve their corresponding transient signals. The details of the analysis and the first ten reconstructed components of SMB and ice discharge are shown in Section S2 of the SM.

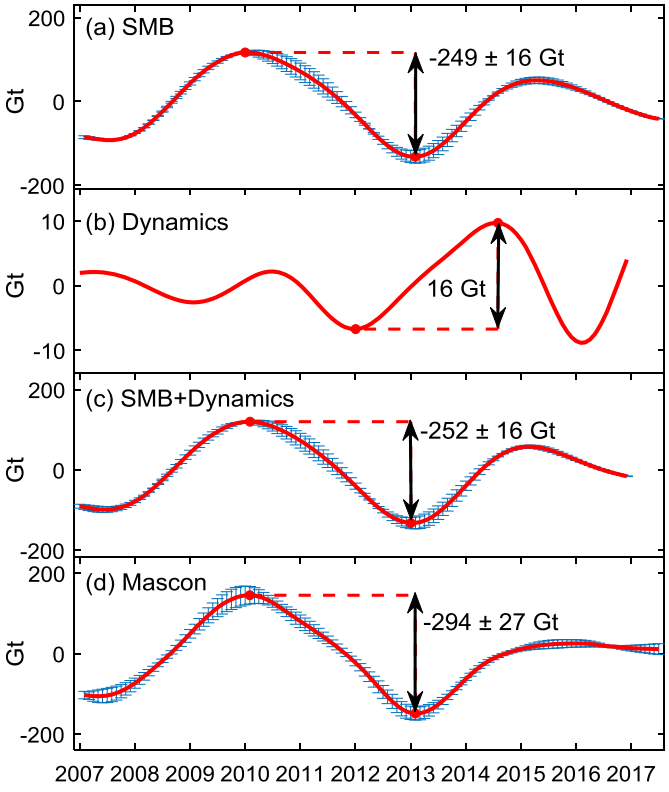

Fig. 2. Transient mass changes of the entire GrIS and its amplitude derived from the SMB data (a), the ice discharge data (b), the sum of SMB and ice discharge (c), and the GRACE mascon data (d). Please note that we use a much narrower vertical range in (b) than in the other three panels for visual clarity.

The M-SSA technique requires that all the time series have the same length and sampling interval, but the time spans of the GPS time series are different. Given this constraint, we only apply SSA (not the 'multichannel' analysis) to each GPS time series at a time to retrieve the transient changes of displacements. The transient signals derived from 26 vertical position time series are presented in Section S3 of the SM.

4. Results

4.1. Transient mass changes of the entire Greenland ice sheet

Fig. 2 shows the transient mass variations of the entire GrIS, extracted from the SMB, dynamics, SMB plus glacial discharge (termed as "SMB+dynamics"), and the mascon data, respectively. The transient signals extracted from the mascon, SMB, and SMB+dynamics data are similar and characterized by a sustained mass gain from late 2007 to early 2010, a sustained mass loss from early 2010 to early 2013, and a mass gain from early 2013 to mid-2015. Based on these time-varying characteristics, we divide the transient mass change into three phases for subsequent investigation, including Phase 1: 2008-2009; Phase 2: 2010-2012; and Phase 3: 2013-2014. We use the peak-to-peak value from early 2010 to early 2013 to quantify the amplitude of the transient variations. The amplitudes are -294 ± 27 Gt and -252 ± 16 Gt for the mascon signal and the SMB+dynamics signal, respectively. The transient signal extracted from the dynamics data shows different patterns with much smaller amplitudes (Fig. 2c). We note that the

magnitude of the dynamic transient changes is about 16 Gt lower than the SMB and mascon amplitudes. The similar time-varying patterns and amplitudes between the SMB and mascon signals suggest that SMB was the dominant contributor to the transient mass change of the GrIS from 2007 to 2017 with little contribution from ice discharge.

We show the long-term and seasonal ice mass changes of the entire GrIS in Section S4 of SM. The long-term ice loss rate and acceleration of the entire GrIS are estimated to be 307.8 ± 11.9 Gt/yr and 18.0 ± 9.3 Gt/yr^2 from 2007 to 2016 based on the JPL mascon solutions with GIA removed by A et al. (2013). The mean peak-to-peak amplitude of the seasonal mass change is estimated to be 136.2 ± 16.3 Gt with amplified amplitudes in 2010-2013. The amplitude of the transient mass change (−294 ± 27 Gt) is comparable to the long-term ice mass loss and is much greater than the seasonal mass change.

To investigate how the transient mass change influences the estimates of the long-term ice change rates, we remove the seasonal oscillations (Fig. S9 of the SM) from the JPL mascon solutions and estimate the ice change rates from 2008 to 2017. The data used for the estimation are accumulated from 2007 to the epoch of interest. After removing the seasonal variations, the changes in the rate estimates are mainly influenced by the transient ice mass variations. Fig. S10 of the SM shows that the estimated ice change rates vary from −237 Gt/yr to −353 Gt/yr and have similar variations as the transient signal (Fig. 2d). This result suggests that the transient variations have a strong influence on the estimates of long-term ice mass loss rates and that the transient mass change is an important component of the ice mass changes in Greenland.

4.2. Transient mass changes of sub-regions

Fig. 3 shows the transient ice mass variations of each subregion, extracted from the SMB, dynamics, their sum, and mascon data. The mascon results (Fig. 3d) reveal that the mass change in CW, SW, SE, and NE show similar patterns as the entire GrIS, but their amplitudes are different: the SE and SW regions have the largest amplitudes (−111 ± 2 Gt), the CW and NE have relatively smaller amplitudes (−34 ± 2 Gt and −46 ± 1 Gt). However, the transient mass changes in the NW and NO have very different signals when compared to the other regions. In these regions, we observe a sustained mass loss from early 2008 to early 2010, a sustained mass gain from early 2010 to early 2013, and a mass loss from early 2013 to 2016. The amplitudes of these signals are small, only 7 ± 2 Gt in the NW and 2 ±1 Gt in the NO. Due to the low signal-to-noise ratio in the NO transient signal, the signal will not be real, and it will not be further interpreted.

The transient signals extracted from the SMB data (Fig. 3a) show similar time varying patterns as those extracted from the mascon data in NW, CW, NE, SW, and SE. Transient signals extracted from dynamics (Fig. 3b) are weak in NO and NE and stronger in NW, CW, SW, and SE. Given the much larger amplitudes of the SMB transient signals in CW, SW, and SE, the dynamic transient signals in these regions contributed little to the total transient mass variations. This result can be observed by comparing Figs. 3a and 3c. However, in NW, the dynamic component contributed significantly to the transient variations by increasing the amplitude of the transient signal from 17 Gt (only SMB, Fig. 3a) to 30 Gt (SMB + dynamics, Fig. 3c), but it only slightly changed the phases of the peaks. Even though the transient signals extracted from the mascon and SMB + dynamics data have different amplitudes (7 Gt vs. 30 Gt) in NW, they show similar phases and time varying patters. Overall, the transient SMB changes reveal similar characteristics to the transient mascon changes, indicating SMB is the main contributor to the transient mass changes in the six subregions. The distributions and amplitudes of the transient mass changes are also summarized in Fig. 4, which indicate that northwest Greenland has different transient mass changes compared to the other regions.

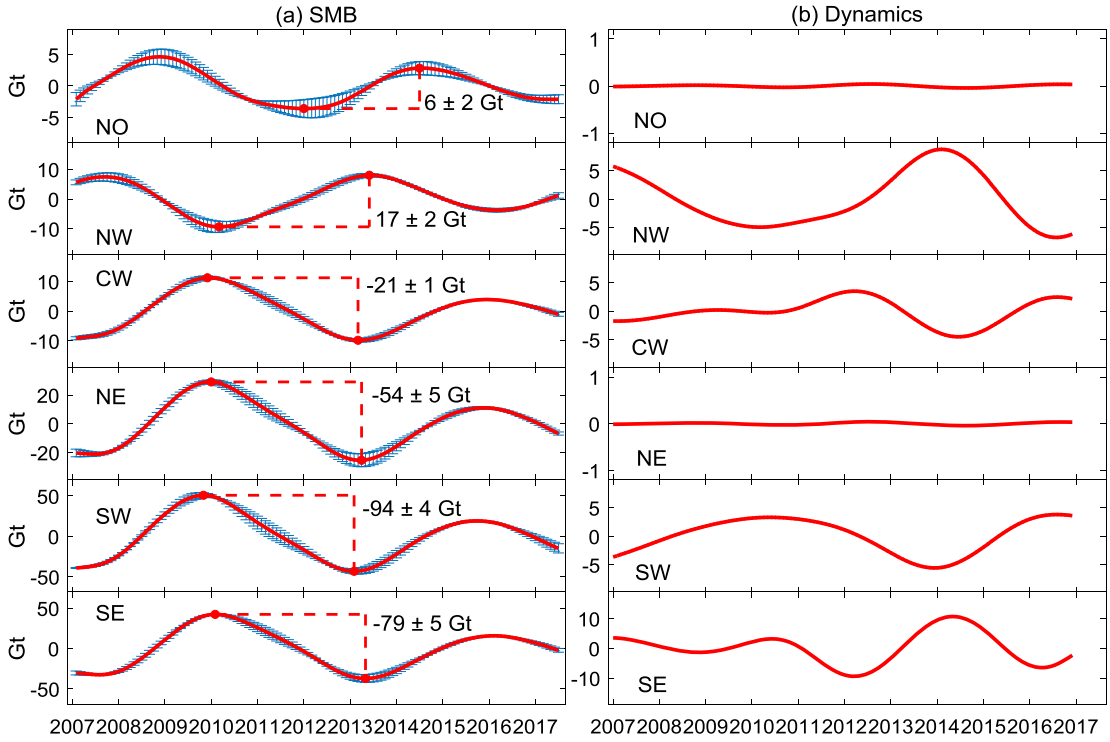

Fig. 3. Transient mass changes within each region, derived from (a) SMB data, (b) ice discharge data, namely ice dynamics, (c) the sum of SMB and ice dynamics, and (d) GRACE mascon data. Note that we use different vertical ranges to visually amplify the temporal patterns.

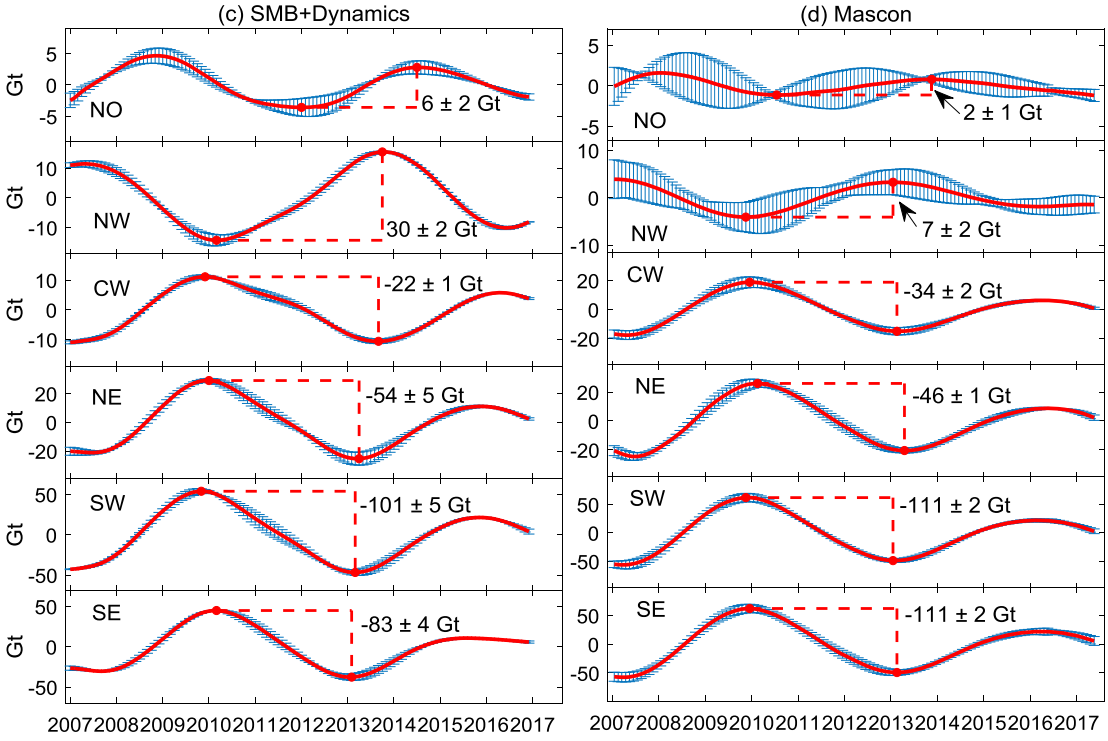

Fig. 3. (*continued*)

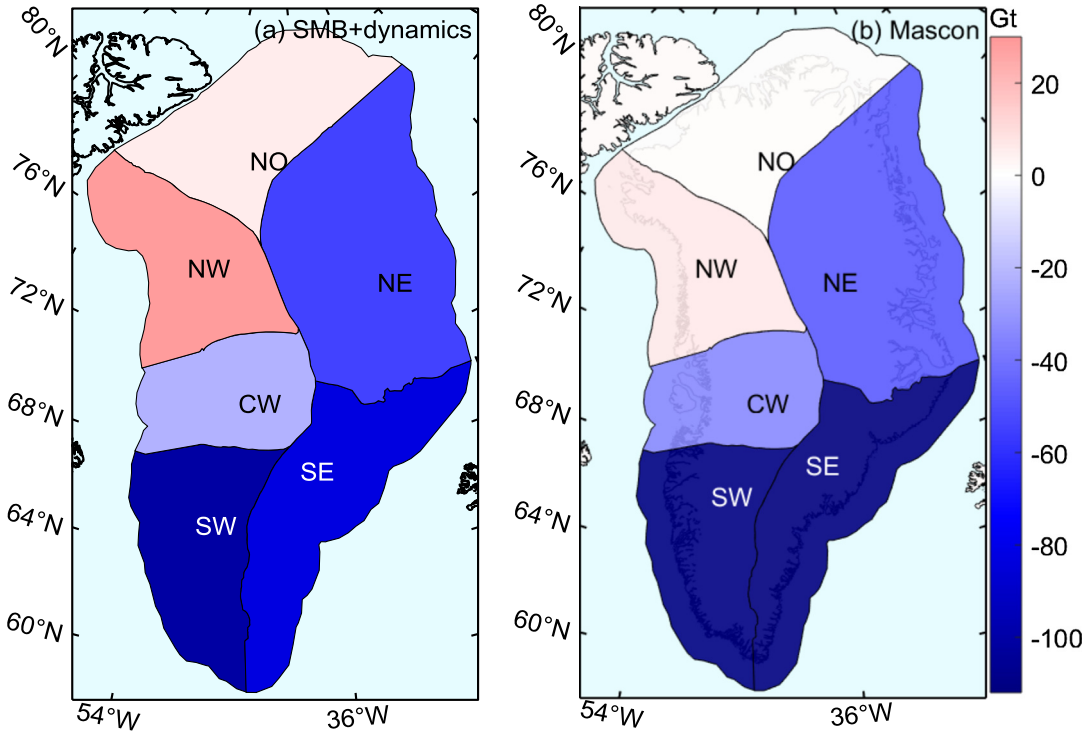

Fig. 4. Amplitudes of transient mass change from 2010 to 2013 of the six sub-regions derived from (a) SMB+dynamics data and (b) GRACE mascon data.

4.3. GPS displacements due to ice mass changes

The transient signals extracted from the 26 GPS vertical position time series are shown in Fig. S7 of the SM. Fig. 5a shows the amplitudes of the transient displacements and Fig. 5b presents the transient displacement time series at five of the 26 sites. Despite site specific local effects associated with the sensitivity of elastic loading to nearby ice mass changes (Wahr et al., 2013; Adhikari et al., 2017; Liu et al., 2017; Zhang et al., 2017), the GPS data share common features. All sites showed uplift from early 2010 to early 2013 and followed by a subsidence from 2013 to around 2015 indicating that more ice mass was lost near the coast of Greenland from around 2010 to 2013, and then followed by less ice mass loss from 2013 to 2015. These displacements were consistent with the transient mass changes of the entire GrIS as shown in Fig. 2. We also find that sites in south Greenland have larger

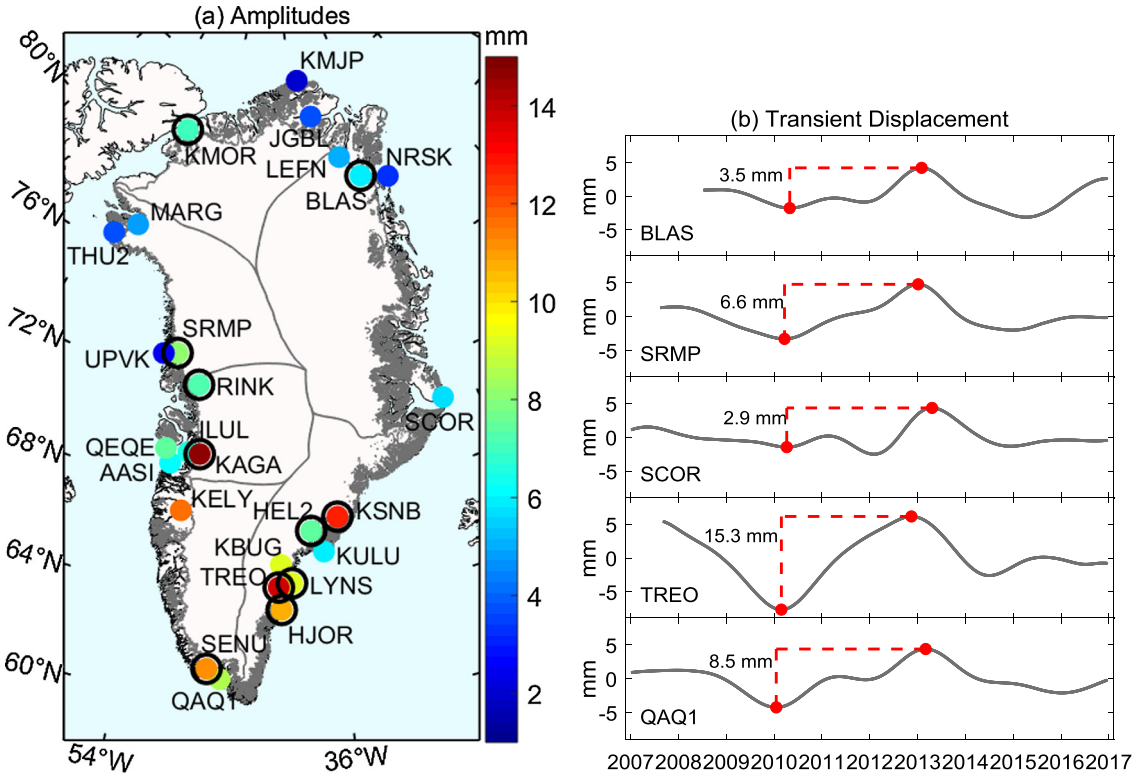

Fig. 5. (a): Amplitudes of the transient displacements from 2010 to 2013 at the 26 GPS sites. Sites with black circles indicate these sites are close to glaciers or ice sheet margins. The peripheral glaciers and ice caps are marked as gray areas. (b): Transient displacements at five exemplary sites.

amplitudes than those in the north (Fig. 5a). This result indicates that the southern coastal regions lost more ice than the northern regions from 2010 to 2013. This is also consistent with the mascon and SMB results as shown in Fig. 4. Fig. 5a shows that 11 sites (KMOR, BLAS, SRMP, RINK, KAGA, KSNB, HEL2, LYNS, TREO, HJOR, and SENU) showed notably larger amplitudes than their nearby sites. This is because these sites are deployed very close to glaciers or ice sheet margins thus capturing a stronger ice loss signal.

5. Discussion

5.1. Transient contributions from runoff and precipitation anomalies

Since SMB was the dominant contributor to the transient mass changes from 2007 to 2016, here we analyze how the runoff and precipitation, the two most important components of SMB, influenced Greenland mass balance in the past decade. To quantify how runoff and precipitation contributed to the transient mass changes, we first calculate the annual anomalies of runoff and precipitation, which are shown in Fig. 6. The anomalies are calculated by removing the 2007-2016 mean from the annual runoff and precipitation. For the entire GrIS (Fig. 6g), the runoff anomalies were much larger than the precipitation anomalies (980 Gt vs. 560 Gt in terms of the summation of the absolute anomalies), which suggests that the runoff anomalies dominated the transient mass changes of the entire GrIS from 2007 to 2016.

We find that the runoff anomalies did not dominate the transient mass changes in all the sub-regions (Fig. 6). During the whole period (2007-2016), runoff contributed more to the transient mass change than precipitation in the NO and SW regions in terms of the summation of the absolute anomalies, less in the NW and NE regions, and comparably in the CW and SE regions.

Moreover, the roles of runoff and precipitation could change in different sub-periods. We compute the average of annual runoff

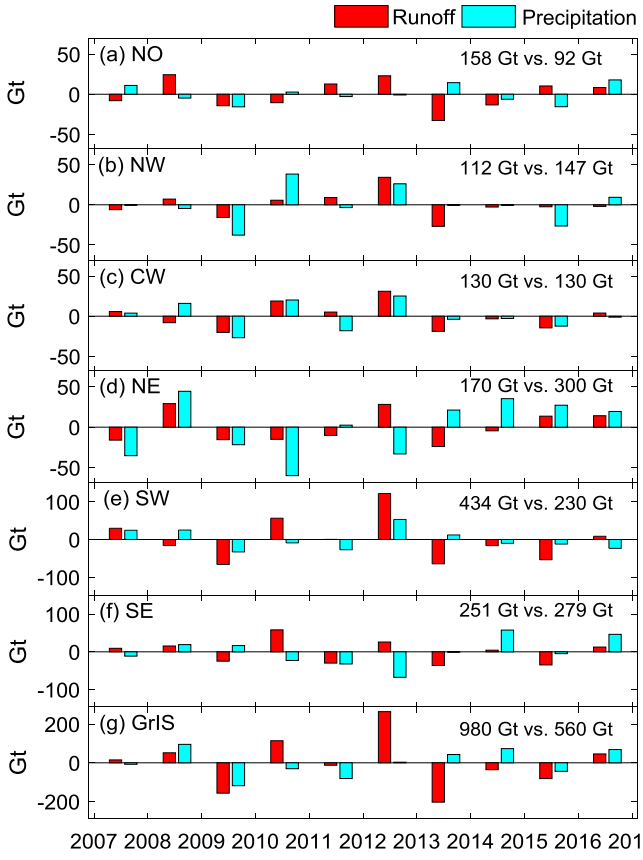

Fig. 6. Annual runoff and precipitation anomalies in the sub-regions (a-f) and the entire GrIS (g) from 2007 to 2016. The numbers in the panels indicate the runoff anomalies versus the precipitation anomalies in terms of the summation of the absolute anomalies from 2007 to 2016.

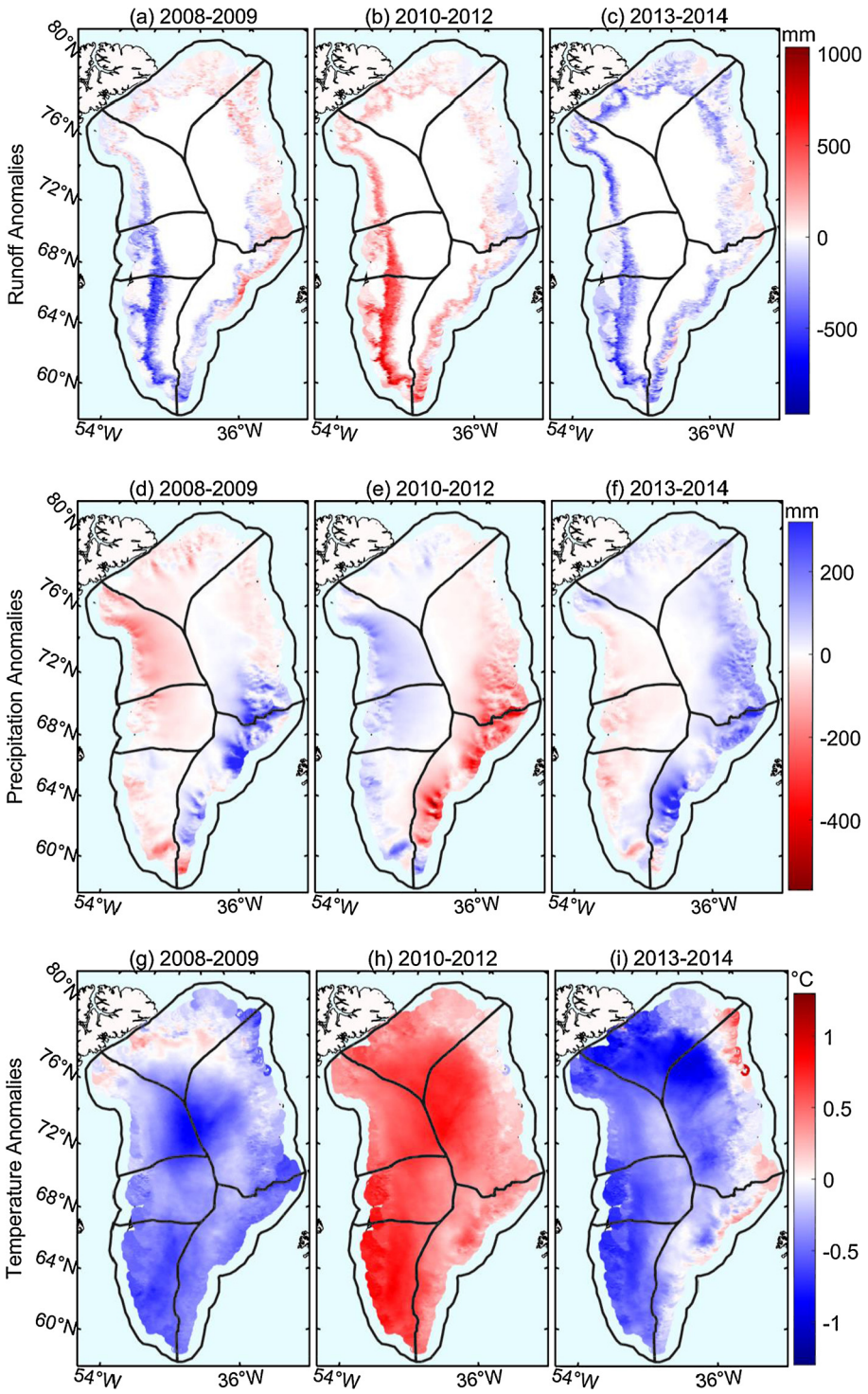

Fig. 7. Average runoff (a-c), precipitation (d-f), and temperature (g-i) anomalies during 2008-2009, 2010-2012, and 2013-2014. Cold/warm colors indicate mass gain/loss shown in panels a-f.

and precipitation anomalies during each phase. These are shown in Fig. 7 in comparison with the temperature anomalies.

Phase 1 (2008-2009):

During this phase, both the runoff and precipitation anomalies were negative in the CW and SW regions (Figs. 7a and 7d). Negative runoff anomalies mean relative mass gain; and vice versa. The sum of these two opposite contributions to ice mass change generated a net mass gain in the CW and SW regions as evidenced in Fig. 3a. This result indicates that the runoff anomalies contributed more to the transient mass change than the precipitation anomalies. In the SE region, it is apparent that the positive precipitation and negative runoff precipitation anomalies together contributed to the transient mass gain during this phase. In the NE region, the positive precipitation anomalies in the south contributed more mass gain than mass loss caused by widespread positive runoff anomalies, finally causing the transient mass gain as shown in Fig. 3a. In the NW and NO regions, it is also apparent from Figs. 7a and 7d that positive runoff and negative precipitation anomalies together contributed to the transient mass loss during this phase.

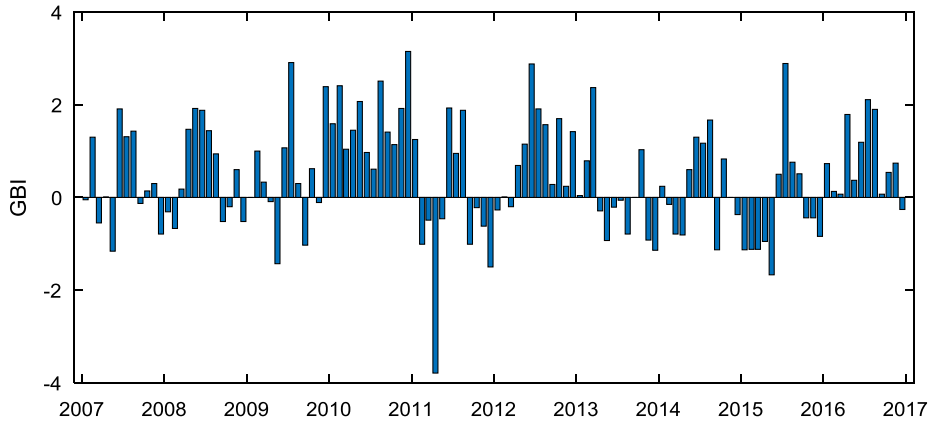

Fig. 8. Time series of monthly Greenland Blocking Index (GBI) anomalies from 2007 to 2016.

Phase 2 (2010-2012):

During this phase, nearly the entire GrIS showed positive runoff anomalies (Fig. 7b) mainly due to two severe melting events that occurred in 2010 (Tedesco et al., 2011) and 2012 (Nghiem et al., 2012; Tedesco et al., 2013). The years 2010 and 2012 were also two of the ten highest-GBI years observed over the period 1851 to 2015 (Hanna et al., 2016). In CW, SW, SE, and NE, runoff dominated the transient mass loss during 2010-2012. However, in the NW and NO regions, the widespread positive precipitation anomalies compensated for the positive runoff anomalies and caused the transient mass gain (Fig. 3a). Fig. 7e also shows that the precipitation anomalies in east and west Greenland were opposite in sign.

Phase 3 (2013-2014):

During this phase, nearly the entire GrIS showed negative runoff anomalies (Fig. 7c) that were opposite to that during phase 1. East Greenland (NO, NE, and SE) showed positive precipitation anomalies while west Greenland (NW, CW, and SW) showed negative precipitation anomalies (Fig. 7c). In east Greenland, negative runoff anomalies and positive precipitation anomalies together contributed to the transient mass gain (Fig. 3a). In the CW and SW regions, the negative runoff anomalies contributed more mass gain than the mass loss caused by negative precipitation anomalies, thus finally generated a transient mass gain (Fig. 3a). In the NW region, the widespread negative precipitation anomalies caused more mass loss than the mass gain contributed from negative runoff anomalies, resulting in a mass loss in the NW (Fig. 3a). Precipitation showed the opposite signs in east and west Greenland.

Since near-surface air temperature is often used as a proxy for surface melting (e.g., Tedesco et al., 2011), we compute the 3-m temperature anomalies from the MAR model during the three phases (Figs. 7g–7i). The temperature anomalies were negative over most of Greenland during phases 1 and 3 but positive during phase 1. By comparing Figs. 7g–7i and Fig. 2, we observe that higher (lower) temperature caused the entire GrIS to lose (gain) more ice mass. Comparing the temperature anomalies with the precipitation anomalies, we also observe that higher (lower) temperature correlated with more (less) precipitation in west Greenland and less in east Greenland.

5.2. Climatologic mechanisms for transient mass changes

The GBI and North Atlantic Oscillation (NAO) index are important atmospheric indices that reflect the state of the general atmospheric circulation over Greenland. The GBI was defined by Fang (2004) based on the mean 500 hPa geopotential height (GPH) for the 60-80°N, 20-80°W region and popularized by Hanna et al. (2013, 2014, 2015, 2016). The NAO index is based on the surface sea-level pressure difference between the Subtropical (Azores) High and the Subpolar Low (Hurrell, 1995). The NAO is associated with atmospheric blocking over GrIS, and both NAO and GBI have influences on the GrIS's ice mass balance (Pattyn et al., 2018). The correlation coefficient between the GBI and Hurrell PC-based NAO index from 2007 to 2016 is −0.87. This high anti-correlation indicates that the GBI and NAO characterize the same atmospheric circulations. Here we use only GBI to explain the transient mass changes over Greenland.

The NAO is most pronounced in winter whereas the transient mass change was mainly caused by summer runoff. GBI correlates more directly with GrIS runoff changes than does the NAO index (Hanna et al., 2013). To be consistent with the relative transient mass changes we reported earlier in Sections 4.1 and 5.1, we remove the 2007-2016 mean from the GBI presented in Hanna et al. (2016) to obtain the "GBI anomalies" (Fig. 8). The three-year-averaged GBI anomalies for 2007-2009, 2010-2012, and 2013-2015 are 0.00, 0.34, and −0.46 (i.e., 2010-2012 was a high-GBI period while 2013-2015 was a low-GBI period).

Temperature anomalies under a high (low)-GBI regime are high (low) over Greenland, partly because the GPH is thermodynamically linked to temperatures (Overland and Wang, 2015; Hanna et al., 2016). The temperature anomalies shown in Figs. 7h and 7i support this conclusion.

Fig. 6 in Hanna et al. (2016) shows that a high-summer-GBI regime is associated with a dipole of precipitation anomalies, less in southeast Greenland, more in the northwest. This can be also observed from Figs. 7e and 7f. The opposite behaviors of precipitation anomalies between the east and west Greenland have also been reported by Bjørk et al. (2018).

During 2010-2012, the high-GBI-associated high temperature caused more ice melting and runoff over nearly the entire GrIS. Though high GBI brought more precipitation in west Greenland, temperature played a dominant role in affecting ice mass loss of the entire GrIS. While in the NW region, the positive precipitation anomaly overcompensated the high temperature induced mass loss and thus resulted in a transient mass gain. During 2013-2015, a low-GBI-associated low temperature caused less ice melting and runoff over nearly the entire GrIS. In contrast, in the NW region, low GBI induced less precipitation and thus contributed to the transient mass loss.

In addition to GBI and NAO that characterize atmospheric, Greenland ice mass loss/gain is also influenced by many other drivers, including other unmodeled atmospheric circulations, ocean-ice sheet interactions, and storms, etc. We are unable to use the GBI or NAO to explain the 2007-2010 transient mass changes since neither the GBI or NAO anomalies were significant during

this period. The relationship between transient mass changes and climatologic drivers is far more complex than one or two atmospheric indices can explain. Here we only demonstrate that in the high or low GBI periods, GBI is correlated with the transient mass changes.

6. Conclusions

We apply M-SSA to the GRACE mascon, SMB, and ice discharge data over Greenland and extract the transient mass changes of the entire GrIS and the six sub-regions. The transient mass change of the entire GrIS is characterized by a sustained relative mass gain from late 2007 to early 2010, followed by a sustained mass loss from early 2010 to early 2013, and a mass gain from early 2013 to mid-2015. The CW, NE, SW, and SE regions showed a time-varying pattern similar to the entire GrIS, but the NO and NW were different. Results obtained from the SMB models and the GPS vertical displacement time series corroborate our findings.

We also find that GBI can largely explain the transient mass changes during the 2010-2012 high GBI period and the 2013-2015 low GBI period. High (Low) -GBI-associated high temperature caused the GrIS to lose more (less) ice. This explained the transient mass loss during 2010-2012 and the transient mass gain during 2013-2015 of the entire GrIS. However, the precipitation anomalies under high or low GBI were opposite in west and east Greenland. This led to the different behaviors of ice mass change in the NW as compared to other regions.

Overall, this study gives insight into the spatio-temporal variations of the transient mass changes over Greenland during the past decade and proposes potential climatological mechanisms to explain these changes. This study highlights the need to improve our understanding of the relationship between atmospheric circulations and short-term Greenland mass balance.

Competing interests

The authors declare to have no conflict of interest.

Acknowledgements

We thank Dr. Xavier Fettweis for providing the MAR surface mass balance data, Prof. Jonathan Bamber for providing the Greenland ice discharge data. We also thank Jet Propulsion Laboratory, Goddard Space Flight Center, and Center for Space Research, University of Texas Austin for providing the Level 2 GRACE data, and the UNAVCO Facility for providing the GPS data. This work was supported by Hong Kong Research Grants Council Grant (CUHK24300414) and by National Natural Science Foundation of China (41704004). S.A.K. was funded in part by Carlsbergfondet (CF14-0145) and the Danish Council for Independent Research (DFF-4181-00126). B.N. acknowledges support from the Polar Programme of the Netherlands Organization for Scientific Research (NWO/ALW) and the Netherlands Earth System Science Centre (NESSC).

Appendix A. Supplementary material

Supplementary material related to this article can be found online at https://doi.org/10.1016/j.epsl.2019.03.028.

References

A, G., Wahr, J., Zhong, S., 2013. Computations of the viscoelastic response of a 3-D compressible Earth to surface loading: an application to Glacial Isostatic Adjustment in Antarctica and Canada. Geophys. J. Int. 192 (2), 557–572.

Adhikari, S., Ivins, E.R., Larour, E., 2017. Mass transport waves amplified by intense Greenland melt and detected in solid Earth deformation. Geophys. Res. Lett. 44, 4965–4975. https://doi.org/10.1002/2017GL073478.

Bamber, J.L., Tedstone, A.J., King, M.D., Howat, I.M., Enderlin, E.M., van den Broeke, M.R., Noel, B., 2018. Land ice freshwater budget of the Arctic and North Atlantic Oceans: 1. Data, methods, and results. J. Geophys. Res., Oceans 123 (3), 1827–1837.

Bjørk, A.A., Aagaard, S., Lütt, A., Khan, S.A., Box, J.E., Kjeldsen, K.K., Machguth, H., et al., 2018. Changes in Greenland's peripheral glaciers linked to the North Atlantic Oscillation. Nat. Clim. Change 8 (1), 48.

Broomhead, D.S., King, G.P., 1986. On the qualitative analysis of experimental dynamical systems. Nonlinear Phenom. Chaos 113, 114.

Cazenave, A., Remy, F., 2011. Sea level and climate: measurements and causes of changes. Wiley Interdiscip. Rev.: Clim. Change 2 (5), 647–662.

Chen, J.L., Wilson, C.R., Tapley, B.D., 2006. Satellite gravity measurements confirm accelerated melting of Greenland ice sheet. Science 313 (5795), 1958–1960.

Chen, J.L., Wilson, C.R., Tapley, B.D., 2011. Interannual variability of Greenland ice losses from satellite gravimetry. J. Geophys. Res., Solid Earth 116 (B7).

Csatho, B.M., Schenk, A.F., van der Veen, C.J., Babonis, G., Duncan, K., Rezvanbehbahani, S., van Angelen, J.H., et al., 2014. Laser altimetry reveals complex pattern of Greenland Ice Sheet dynamics. Proc. Natl. Acad. Sci. USA 111 (52), 18478–18483.

Fang, Z.F., 2004. Statistical relationship between the northern hemisphere sea ice and atmospheric circulation during wintertime. In: Observation, Theory and Modeling of Atmospheric Variability: Selected Papers of Nanjing Institute of Meteorology Alumni in Commemoration of Professor Jijia Zhang, pp. 131–141.

Farrell, W.E., 1972. Deformation of the Earth by surface loads. Rev. Geophys. 10 (3), 761–797.

Fettweis, X., Box, J., Agosta, C., Amory, C., Kittel, C., Lang, C., Gallée, H., et al., 2017. Reconstructions of the 1900–2015 Greenland ice sheet surface mass balance using the regional climate MAR model. Cryosphere 11, 1015–1033.

Hanna, E., Jones, J.M., Cappelen, J., Mernild, S.H., Wood, L., Steffen, K., Huybrechts, P., 2013. The influence of North Atlantic atmospheric and oceanic forcing effects on 1900–2010 Greenland summer climate and ice melt/runoff. Int. J. Climatol. 33 (4), 862–880.

Hanna, E., Fettweis, X., Mernild, S.H., Cappelen, J., Ribergaard, M.H., Shuman, C.A., Mote, T.L., et al., 2014. Atmospheric and oceanic climate forcing of the exceptional Greenland ice sheet surface melt in summer 2012. Int. J. Climatol. 34 (4), 1022–1037.

Hanna, E., Cropper, T.E., Jones, P.D., Scaife, A.A., Allan, R., 2015. Recent seasonal asymmetric changes in the NAO (a marked summer decline and increased winter variability) and associated changes in the AO and Greenland blocking index. Int. J. Climatol. 35 (9), 2540–2554.

Hanna, E., Cropper, T.E., Hall, R.J., Cappelen, J., 2016. Greenland blocking index 1851–2015: a regional climate change signal. Int. J. Climatol. 36 (15).

Hurrell, J.W., 1995. Decadal trends in the North Atlantic Oscillation: regional temperatures and precipitation. Science 269 (5224), 676–679.

Khan, S.A., Liu, L., Wahr, J., Howat, I., Joughin, I., van Dam, T., Fleming, K., 2010. GPS measurements of crustal uplift near Jakobshavn Isbræ due to glacial ice mass loss. J. Geophys. Res., Solid Earth 115 (B9).

Khan, S.A., Kjær, K.H., Bevis, M., Bamber, J.L., Wahr, J., Kjeldsen, K.K., Liu, L., et al., 2014. Sustained mass loss of the northeast Greenland ice sheet triggered by regional warming. Nat. Clim. Change 4 (4), 292.

Khan, S.A., Sasgen, I., Bevis, M., van Dam, T., Bamber, J.L., Wahr, J., Csatho, B., et al., 2016. Geodetic measurements reveal similarities between post–Last Glacial Maximum and present-day mass loss from the Greenland ice sheet. Sci. Adv. 2 (9), e1600931.

Kjeldsen, K.K., Korsgaard, N.J., Bjørk, A.A., Khan, S.A., Box, J.E., Funder, S., Siggaard-Andersen, M.L., et al., 2015. Spatial and temporal distribution of mass loss from the Greenland Ice Sheet since AD 1900. Nature 528 (7582), 396–400.

Liu, L., Khan, S.A., Dam, T., Ma, J.H.Y., Bevis, M., 2017. Annual variations in GPS-measured vertical displacements near Upernavik Isstrøm (Greenland) and contributions from surface mass loading. J. Geophys. Res., Solid Earth 122 (1), 677–691.

Luthcke, S.B., Sabaka, T.J., Loomis, B.D., Arendt, A.A., McCarthy, J.J., Camp, J., 2013. Antarctica, Greenland and Gulf of Alaska land-ice evolution from an iterated GRACE global mascon solution. J. Glaciol. 59 (216), 613–631.

Nghiem, S.V., Hall, D.K., Mote, T.L., Tedesco, M., Albert, M.R., Keegan, K., Neumann, G., et al., 2012. The extreme melt across the Greenland ice sheet in 2012. Geophys. Res. Lett. 39 (20).

Noël, B., van de Berg, W.J., Wessem, V., Melchior, J., van Meijgaard, E., van As, D., Lenaerts, J.T.M., Lhermitte, S., Munneke, P.K., Smeets, C.J.P., van Ulft, L.H., van de Wal, R.S.W., van den Broeke, M.R., 2018. Modelling the climate and surface mass balance of polar ice sheets using RACMO2-Part 1: Greenland (1958-2016). Cryosphere 12 (3), 811–831.

Overland, J.E., Wang, M., 2015. Increased variability in the early winter subarctic North American atmospheric circulation. J. Climate 28 (18), 7297–7305.

Pattyn, F., Ritz, C., Hanna, E., Asay-Davis, X., DeConto, R., Durand, G., Favier, L., Fettweis, X., Goelzer, H., Golledge, N.R., Munneke, P.K., Lenaerts, J.T.M., Nowicki, S., Payne, A.J., Robinson, A., Seroussi, H., Trusel, L.D., van den Broeke, M., 2018. The Greenland and Antarctic ice sheets under 1.5 °C global warming. Nat. Clim. Change 8, 1053–1061.

Ramillien, G., Lombard, A., Cazenave, A., Ivins, E.R., Llubes, M., Remy, F., Biancale, R., 2006. Interannual variations of the mass balance of the Antarctica and Greenland ice sheets from GRACE. Glob. Planet. Change 53 (3), 198–208.

Rangelova, E., Sideris, M.G., Kim, J.W., 2012. On the capabilities of the multi-channel singular spectrum method for extracting the main periodic and non-periodic variability from weekly GRACE data. J. Geodyn. 54, 64–78.

Rignot, E., Box, J.E., Burgess, E., Hanna, E., 2008. Mass balance of the Greenland ice sheet from 1958 to 2007. Geophys. Res. Lett. 35, L20502. https://doi.org/10.1029/2008GL035417.

Rignot, E., Velicogna, I., Van Den Broeke, M.R., Monaghan, A., Lenaerts, J., 2011. Acceleration of the contribution of the Greenland and Antarctic ice sheets to sea level rise. Geophys. Res. Lett. 38 (5). https://doi.org/10.1029/2011GL046583. L05503.

Sasgen, I., van den Broeke, M., Bamber, J.L., Rignot, E., Sørensen, L.S., Wouters, B., Simonsen, S.B., et al., 2012. Timing and origin of recent regional ice-mass loss in Greenland. Earth Planet. Sci. Lett. 333, 293–303.

Save, H., Bettadpur, S., Tapley, B.D., 2016. High-resolution CSR GRACE RL05 mascons. J. Geophys. Res., Solid Earth 121 (10), 7547–7569.

Seo, K.W., Waliser, D.E., Lee, C.K., Tian, B., Scambos, T., Kim, B.M., van den Broeke, M.R., et al., 2015. Accelerated mass loss from Greenland ice sheet: links to atmospheric circulation in the North Atlantic. Glob. Planet. Change 128, 61–71.

Shepherd, A., Ivins, E.R., Geruo, A., Barletta, V.R., Bentley, M.J., Bettadpur, S., Horwath, M., et al., 2012. A reconciled estimate of ice-sheet mass balance. Science 338 (6111), 1183–1189.

Tedesco, M., Fettweis, X., Van den Broeke, M.R., Van de Wal, R.S.W., Smeets, C.J.P.P., van de Berg, W.J., Box, J.E., et al., 2011. The role of albedo and accumulation in the 2010 melting record in Greenland. Environ. Res. Lett. 6 (1), 014005.

Tedesco, M., Fettweis, X., Mote, T., Wahr, J., Alexander, P., Box, J.E., Wouters, B., 2013. Evidence and analysis of 2012 Greenland records from spaceborne observations, a regional climate model and reanalysis data. Cryosphere 7 (2), 615.

van den Broeke, M., Bamber, J., Ettema, J., Rignot, E., Schrama, E., van de Berg, W.J., Wouters, B., et al., 2009. Partitioning recent Greenland mass loss. Science 326 (5955), 984–986.

Velicogna, I., Wahr, J., Hanna, E., Huybrechts, P., 2005. Short term mass variability in Greenland, from GRACE. Geophys. Res. Lett. 32 (5).

Velicogna, I., Wahr, J., 2006. Acceleration of Greenland ice mass loss in spring 2004. Nature 443 (7109), 329.

Velicogna, I., 2009. Increasing rates of ice mass loss from the Greenland and Antarctic ice sheets revealed by GRACE. Geophys. Res. Lett. 36 (19).

Wahr, J., Khan, S.A., Dam, T., Liu, L., Angelen, J.H., Broeke, M.R., Meertens, C.M., 2013. The use of GPS horizontals for loading studies, with applications to northern California and southeast Greenland. J. Geophys. Res., Solid Earth 118 (4), 1795–1806.

Walwer, D., Calais, E., Ghil, M., 2016. Data-adaptive detection of transient deformation in geodetic networks. J. Geophys. Res., Solid Earth 121, 2129–2152. https://doi.org/10.1002/2015JB012424.

Watkins, M.M., Wiese, D.N., Yuan, D.N., Boening, C., Landerer, F.W., 2015. Improved methods for observing Earth's time variable mass distribution with GRACE using spherical cap mascons. J. Geophys. Res., Solid Earth 120 (4), 2648–2671.

Wiese, D.N., 2015. GRACE Monthly Global Water Mass Grids NetCDF Release 5.0. Ver. 5.0. PO.DAAC, CA, USA. https://doi.org/10.5067/TEMSC-OCL05. (Accessed 1 October 2017).

Wouters, B., Chambers, D., Schrama, E.J.O., 2008. GRACE observes small-scale mass loss in Greenland. Geophys. Res. Lett. 35 (20).

Wu, X., Heflin, M.B., Ivins, E.R., Fukumori, I., 2006. Seasonal and interannual global surface mass variations from multisatellite geodetic data. J. Geophys. Res., Solid Earth 111 (B9).

Zhang, B., Liu, L., Khan, S.A., van Dam, T., Zhang, E., Yao, Y., 2017. Transient variations in glacial mass near Upernavik Isstrøm (west Greenland) detected by the combined use of GPS and GRACE data. J. Geophys. Res., Solid Earth 122 (12).

Zhang, B., Zhang, E., Liu, L., Khan, S.A., van Dam, T., Yao, Y., Bevis, M., Helm, V., 2018. Geodetic measurements reveal short-term changes of glacial mass near Jakobshavn Isbræ (Greenland) from 2007 to 2017. Earth Planet. Sci. Lett. 503, 216–226.

Zwally, H.J., Li, J., Brenner, A.C., Beckley, M., Cornejo, H.G., DiMarzio, J., Yi, D., et al., 2011. Greenland ice sheet mass balance: distribution of increased mass loss with climate warming; 2003–07 versus 1992–2002. J. Glaciol. 57 (201), 88–102.